Brain Pathology ISSN 1015–6305

REVIEW

# Advances in drug delivery to high grade gliomas

Guido Frosina

Mutagenesis Unit, IRCCS Azienda Ospedaliera Universitaria San Martino - IST Istituto Nazionale per la Ricerca sul Cancro, Genova, Italy.

**Keywords**
blood brain barrier, blood tumor barrier, convection-enhanced delivery, Ommaya reservoir, polymeric depot.

**Corresponding author:**
Guido Frosina, PhD, Mutagenesis Unit, IRCCS Azienda Ospedaliera Universitaria San Martino - IST Istituto Nazionale per la Ricerca sul Cancro, Largo Rosanna Benzi 10, 16132 Geneva, Italy (E-mail: *guido.frosina@hsanmartino.it*)

Received 20 June 2016
Accepted 19 July 2016
Published Online Article Accepted 2 August 2016

doi:10.1111/bpa.12423

## Abstract

If cancer is hard to be treated, brain cancer is even more, caused by the inability of many effective drugs given systemically to cross the blood brain and blood tumor barriers and reach adequate concentrations at the tumor sites. Effective delivery of drugs to brain cancer tissues is thus a necessary, albeit not sufficient, condition to effectively target the disease. In order to analyze the current status of research on drug delivery to high grade gliomas (HGG-WHO grades III and IV), the most frequent and aggressive brain cancers, a literature search was conducted in PubMed using the terms: "drug delivery and brain tumor" over the publication year 2015. Currently explored drug delivery techniques for HGG include the convection and permeabilization-enhanced deliveries, drug-releasing depots and Ommaya reservoirs. The efficacy/safety ratio widely varies among these techniques and the success of current efforts to increase this ratio widely varies as well.

## HIGH GRADE GLIOMAS: TWICE AS DIFFICULT

Despite a multimodal therapeutic approach involving a combination of surgery, radiotherapy and adjuvant chemotherapy, the prognosis of patients with high grade gliomas (HGG, WHO grades III and IV) remains poor (38). Therapeutic failures have often been attributed to the inability of drugs to cross the blood brain barrier (BBB), a major obstacle preventing adequate concentrations of chemotherapeutics being reached in tumor tissues. The BBB, comprised of endothelial efflux transporters as well as brain endothelial cells with tight junctions between them, regulates the extravasation of molecules and cells into and out of the central nervous system (CNS) (8). While metabolic substrates like carbohydrates and aminoacids are able to traverse the BBB by specific carrier-mediated transport systems like glucose transporters present on both the luminal and abluminal side of the BBB (46) many therapeutics such as mostly available cytotoxic drugs that are large hydrophobic molecules or antibody-based proteins, have limited permeability and do not cross the BBB (4). Merely to quote a few examples, anthracyclines show potent effects in inhibiting cell growth in many types of tumors but they suffer from a poor penetration into the brain when intravenously administered (45). The *in vivo* efficacy of MK-1775, a specific inhibitor of the nuclear kinase Wee1 that regulates key DNA damage checkpoints, is limited by poor delivery to the tumor: MK-1775 is ineffective when combined with temozolomide (TMZ) in treatment of brain tumors, whereas in a flank model of HGG, MK-1775 exhibits both single-agent and combinatorial activity with TMZ (44). The combination of the PARP inhibitor rucaparib with TMZ may significantly prolong the time to tumor regrowth by 40% in heterotopic xenografts while the addition of rucaparib has no impact on the efficacy of TMZ in orthotopic models (40, 41). Matrix-assisted laser desorption/ionization (MALDI) mass spectrometric (MS) imaging demonstrated significantly enhanced accumulation of drug in flank tumor compared with normal brain or orthotopic tumors (40, 41). A blood tumor barrier (BTB) may encompass as well the existing and newly formed blood vessels that deliver nutrients and oxygen to the tumor and facilitate HGG cell migration to other parts of the brain. Even though the BTB may be "leaky" in the core part of some HGG, it often closely resembles the intact BBB and prevents efficient passage of cancer therapeutics, including small molecules and antibodies. Thus, many drugs are blocked from reaching the infiltrative glioma-initiating cells (GIC) that are responsible for "within-organ-metastases" away from the core part of the tumor and effective drug delivery to the widespread tumor infiltrations remains challenging because of this as well as other factors such as the increased interstitial pressure. The problem of drugs not reaching the tumor sites relates to brain metastases as well [eg, from breast cancer (BCBM)] (37).

Critical insights into the composition and function of the BBB have been recently reviewed (8). A better understanding of BBB physiology along with the development of new technologies recently allowed for innovative methods to circumvent this barrier (42). The numerous ongoing studies for drug delivery to HGG including convection-enhanced delivery and drug-releasing

membranes as well as technologies that may lead to transient BBB disruption thus allowing for more effective drug crossing to the brain will be discussed (4). Nanoparticle (NP)-mediated drug delivery to HGG has been dealt with elsewhere (21) and will not be included here unless NP were delivered by one of the above techniques (48).

## CONVECTION-ENHANCED DELIVERY

Preclinical studies and the most prominent clinical trials of convection-enhanced delivery (CED) in the treatment of HGG have been recently reviewed (28). CED enables continuous local drug delivery to the CNS for a number of antitumor agents which would normally be excluded by the BBB and BTB (26). Intracranial drug administration via CED may also potentially overcome systemic toxicities. Randomized trials of CED therapy have not yet shown so far survival advantages as compared with standard of care. However, early studies may have been limited by "first generation" delivery techniques and recently reported improvements may potentially allow for better outcomes (26). In particular, catheter design and placement-in are critical components of any CED protocol (34). An intraoperative magnetic resonance imaging (MRI)-compatible system has been developed for direct placement of CED cannulae using real-time imaging (Figure 1A) (15). Patients underwent intraoperative MRI-guided placement of six CED infusion cannulae each, for treatment of diffuse intrinsic brainstem glioma or Parkinson's disease. Convective infusion cannulae were guided to the target using an intraoperative MRI-based navigation platform (developed by MRI Interventions, Inc. http://www.mriinterventions.com/). Fine adjustments were made with x- and y-axis offset controls. Real-time intraoperative MRI during infusion cannula insertion allowed for monitoring of trajectory accuracy during placement. The mean radial, anteroposterior, lateral and tip (distance between the planned target and actual tip) errors were remarkably all lower than 2 mm. Surprisingly, there was no correlation between the length of the planned trajectory and any of the measured errors. No complications were associated with cannula placement indicating that real-time intraoperative MRI-based targeting and monitoring of infusion cannula placement may be safe and effective. Coupled with computational methods allowing a better determination of the biodistribution of the infusate (34), the above cannula insertion procedures may improve the thoroughness of CED for HGG treatment (15).

Brain-penetrating NP incorporating superparamagnetic iron oxide (SPIO) and capable of penetrating brain tissue and distribute over clinically relevant volumes when administered via CED have been developed (Figure 1B) (48). After CED, the distribution of SPIO-NP in the brain could be detected as hypointensities using MRI, the volume occupied by the brain-penetrating SPIO NP increased when the SPIO NP dose was increased and their signal lasted over 1 month (48). Administration of SPIO-loaded NP in the clinical setting may thus allow for easier monitoring of NP distribution in the brain. Expression of the epidermal growth factor receptor (EGFR) deletion variant EGFRvIII is one mechanism of radiation and chemotherapy resistance in patients with HGG. EGFRvIII-targeting antibodies such as cetuximab when bioconjugated to SPIO NP (cetuximab-SPIO NP), may simultaneously provide sensitive cancer cell detection by MRI and targeted therapy of experimental HGG (10). Cetuximab-SPIO NP may additionally allow for some radiosensitivity enhancement. An increase in overall survival of nude mice implanted with human HGG xenografts was found after CED of cetuximab-SPIO NP followed by fractionated IR (10). CED of carboplatin has been investigated for the treatment of HGG in both adults and children. Initial results showed yet that carboplatin was associated with neurotoxicity at high infused concentrations in pre-clinical models and intermittent infusions were required because of rapid clearance of carboplatin from the brain. In order to circumvent these problems, carboplatin has been encapsulated in lactic acid–glycolic acid copolymer (PLGA) NP that may confer to this treatment increased tumor cytotoxicity, reduced neuronal toxicity and prolonged tissue half-life (2). CED of nanoliposomes containing the topoisomerase I inhibitor irinotecan (CPT-11) and intraperitoneal treatment with the PI3K/AKT/mTOR pathway inhibitor rapamycin have been combined for HGG therapy. The combination presented some efficacy in a survival study of rodents bearing orthotopic xenografts without rise in toxicity (36). SN-38 is the active metabolite of CPT-11. Novel SN-38-loaded polymeric micelle termed NK012 have been delivered by CED (62). The distribution and local toxicity after CED delivery of NK012 and free SN-38 were evaluated *in vivo*. Histological examination revealed minimum brain tissue damage in rat brains after delivery of NK012 but severe damage with free SN-38 at the same dose. Some efficacy of NK012 delivered via CED was observed in 9L and U87 rodent orthotopic brain tumor models and volumes of NK012 distribution evaluated by histology and contrast-enhanced MRI were consistent (62). Overexpression of galectin-1 by tumor cells may contribute to HGG resistance (17). The effect of local administration by CED of anti-EGFR and anti-galectin-1 siRNA administered separately or in combination on the survival of nude mice bearing orthotopic U87 HGG and on the EGFR and galectin-1 expression in excised U87 tumor tissues have been evaluated. Both siRNA were carried by chitosan lipid NP. Survival of mice bearing orthotopic U87 GB treated by a combination of anti-EGFR and anti-galectin-1 siRNA and TMZ was increased compared to animals treated by single anti-EGFR or anti-galectin-1 siRNA carried by chitosan lipid NP. Decreased EGFR and galectin-1 expressions at the protein level in excised U87 tumor tissues were visualized in parallel by immunofluorescence (17).

To specifically target the highly malignant GIC, new radiotherapeutic procedures are being developed. This is based on the idea that the resistance of HGG to radiation (that is toxic to proliferating cells only) is linked to quiescence of GIC, in turn mediated by constitutive activation of the ataxia telangiectasia mutated (ATM) protein acting as a cell cycle blocker (5). ATM inhibitors such as KU60019 appear to induce proliferation in residual, resistant GIC thus making them sensitive to radiotherapy (51). The KU60019 diffusion and elimination from the animal body and brain, its effects on orthotopic HGG and efficacy toward pediatric GIC have been recently described in a preclinical setting (Figure 1C) (52). Healthy mice were infused by CED with KU60019 and the drug kinetics followed by HPLC/MS on extracts of different brain regions. Already at the end of CED (time after CED 0 h), KU60019 had diffused from the injection site to the ipsilateral and to a lower extent, contralateral hemisphere. Twenty-four hour later, no drug could be detected all over the brain or in other organs, indicating rapid draining and excretion. KU60019 stimulated proliferation of orthotopic HGG cells with the highest effect observed 96 h after drug delivery. Consistently, the highest radiosensitizing effect was observed 96 h after delivery of KU60019 to GIC (52). ATM inhibition may thus

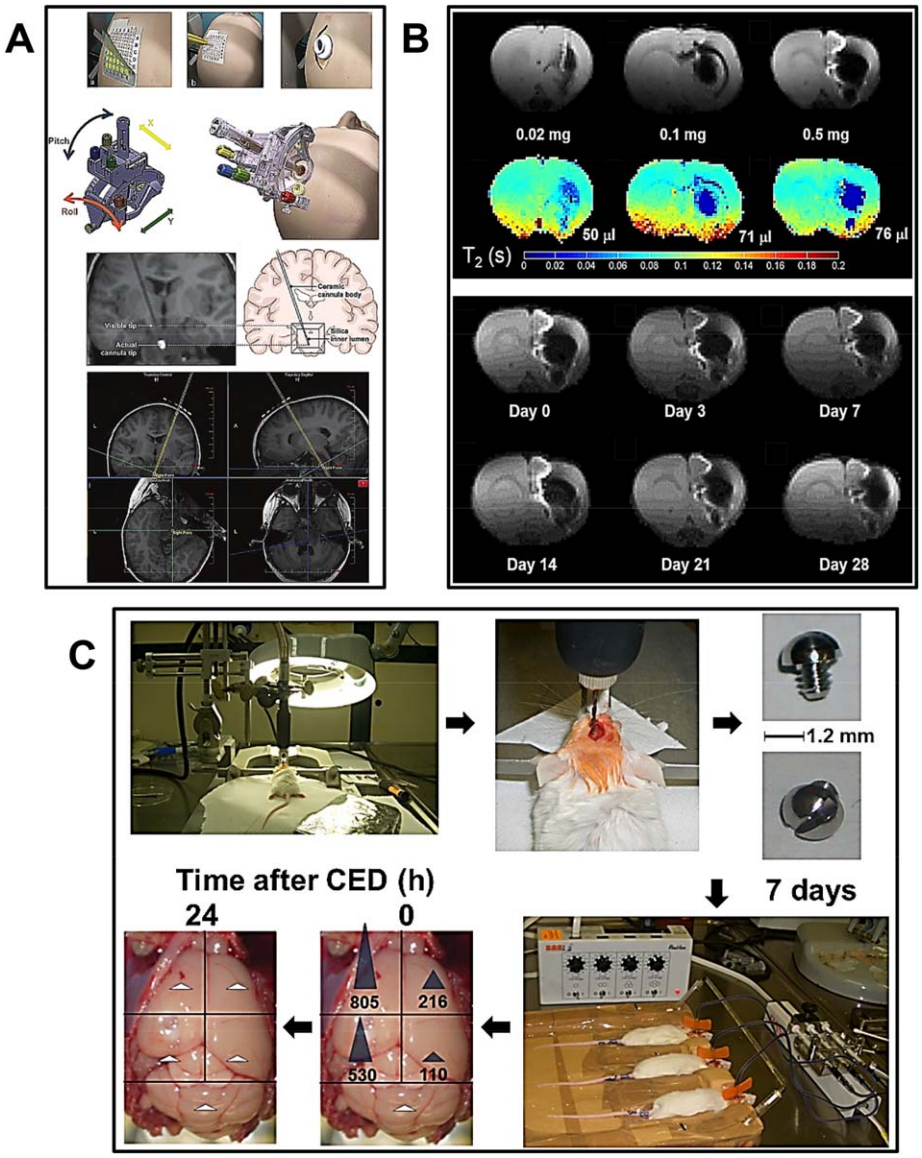


**Figure 1.** Advances in CED. **A.** First row: the outer layer of the grid is peeled off (i) and a mark is made with an augur at the selected site (ii). A bur hole is made after making a parasagittal incision (iii). Second row: the SmartFrame is then attached to the outer table (ii). Large adjustments are made with pitch and roll controls (i). Courtesy of MRI Interventions Inc. Memphis, TN, with permission. Third row: location of the visible tip at the distal end of the ceramic cannula body (ii). The silica inner lumen is not visible on MRI (i) but is visualized at the start of the infusion. Fourth row: using the known entry and target points, the planned trajectory is calculated by the software. In this step, the trajectory is denoted by double yellow lines. A = anterior; H = head (superior); L = left. After Ref. 15, with permission. **B.** (top panel) First row: dose-dependent MR hypointensity of SPIO-loaded brain penetrating NP. Immediately after CED of 20 µL brain-penetrating NP loaded with either 0.02 mg (i), 0.1 mg (ii) or 0.5 mg (iii) SPIO, a series of spin-echo MR images were acquired at 4.0 T. The corresponding T2 MRI maps were also calculated for these three doses (second row). The spin-echo images (first row) showed proportion with the corresponding T2 maps (second row). (bottom panel) First and second rows: MR Images at 4.0 T showing gradual loss of SPIO-loaded brain-penetrating NP with time. Examples of MR images from the same animal scanned at various time points between 0 and 28 days (indicated below each image) following CED of 20 µL of brain-penetrating NP containing 0.5 mg SPIO. The results indicate a slow decrease of the SPIO volume over the time period investigated (after Ref. 48 with permission). **C.** Biodistribution of ATM inhibitor KU60019 intracranially delivered by CED in mice. From top left clockwise, as indicated by arrows: (i, ii) a 1.2-mm burr hole was made in the skull of healthy mice using a flexible shaft drill 2.5 mm lateral and 1-mm anterior to the bregma; (iii, iv) a guide screw with a central hole was inserted into the skull hole to facilitate drug infusion and the incision closed using metal staples; (v) seven days later, 12.5 µL of 250 µM KU60019 in PBS were directly infused into the tumor via a cannula inserted into the guide-screw by CED using an electric micropump set at rate of 0.5 µL/minute; (vi, vii) mice were then euthanized at the end of CED (time after CED 0 h) or 24 h later (time after CED 24 h) and brains explanted and sectioned for analysis of KU60019 biodistribution by HPLC/MS. Blue arrows: KU60019 concentration values higher than limit of quantitation (LOQ - 5 nM). White arrows: KU60019 concentration values lower than LOQ (after Ref. 52 with permission).

allow to radiosensitize both adult and pediatric HGG. Carboranyl-containing chlorins have been proposed as sensitizers for both photodynamic therapy (PDT) and boron neutron capture therapy (BNCT) by virtue of their tumor affinity, low cytotoxicity in dark conditions and absorptions in the red region of the optical spectrum (27). In particular, the applicability of tetrakis(p-carboranylthio-tetrafluorophenyl)chlorin (TPFC), a new synthetic carboranyl-containing chlorin of high boron content as dual sensitizer for both PDT and BNCT has been described after CED in rats bearing F98 orthotopic brain tumors (27). A novel *in situ* permeation (ISP) system for achieving improved intratissue drug diffusion has been proposed and compared to conventional CED (55). The ISP system includes a perfusion catheter connected to an injector and aspirator, which enables intratissue perfusion of the solute diluted in the vehicle. The underlying idea is that when keeping the cavity pressure periodically negative, the focal diffusion of the infused agents may be more controllable. Although the utility of the ISP system for *in situ* permeation was clear in a subcutaneous tumor hamster model, the results of this study have not been confirmed in orthotopic HGG tumors (55).

## PERMEABILIZATION-ENHANCED BRAIN DELIVERY

HGG multimodality imaging include T1-gadolinium contrast-enhanced MR (T1-GAD) that may yet be limited in detecting only the core tumor mass where the BBB is disrupted and cannot detect invasive glioma cells in surrounding areas where the BBB remains intact (Figure 2A, central panels) (7). Alternatively, $^{18}$F-DOPA PET (Figure 2A, right panels) and T2-weighted fluid attenuated inversion recovery (T2-FLAIR) MR scans (Figure 2A, left panels) delineate a larger volume of tumor than T1-GAD in the same patients, thus allowing to visualize tumor regions with an intact BBB. P-glycoprotein (P-GP) and breast cancer resistance protein (BCRP) have been identified as BBB-associated efflux transporters. To test the hypothesis that efflux transporters influence brain PK/PD of molecularly targeted agents in HGG treatment, the region-specific penetrance and molecular-targeting capacity for a PI3K/mTOR kinase inhibitor that has substrate affinity for efflux transporters (GDC-0980) and an analog (GNE-317) that was purposely designed to have reduced efflux have been investigated (7). Animals treated with GNE-317 demonstrated threefold greater penetrance in tumor core, rim and normal brain compared with animals dosed with GDC-0980 and its increased brain penetrance correlated with decreased activation of p-Akt, p-S6 and p-4EBP1 effector proteins downstream of PI3K and mTOR. GDC-0980 may be subject to active efflux by P-GP and BCRP at the BBB, while brain penetrance of GNE-317 is independent of efflux, which translates into enhanced inhibition of PI3K/mTOR signaling suggesting that BBB efflux by P-GP and BCRP may influence both brain penetrance and molecular targeting efficacy (7). The effect of ultrasound-induced BBB opening on the intracerebral concentration of TMZ and CPT-11 has been assessed in rabbits (6). The mean intracerebral tissue-to-plasma drug concentration ratio in the control hemispheres was 34% for TMZ and 2% for CPT-11. After BBB opening, these values increased 1.37 and 2.70-fold for TMZ and CPT-11, respectively. Intracerebral concentrations of drugs were enhanced in regions where the BBB was opened compared with the contralateral hemisphere and the control group but the absolute delivery values for CPT-11 remained relatively modest after ultrasound opening (maximal brain value concentration: 238 ng/g) and no enhanced tumor control was shown (6). The opening of the tight junctions in the BBB following traumatic (eg, surgical) brain injury (TBI) is hypothesized to be sufficient to enable accumulation of large drug carriers such as liposomes. The controlled cortical model of TBI was used to evaluate liposome accumulation in mice. Dual-radiolabeled PEGylated liposomes were administered either immediately after induction of TBI or at increasing times post-TBI. Selective influx of liposomes occurred at 0–8 h after injury, while the barrier closed between 8 and 24 h after injury, consistent with reports on albumin infiltration. Significantly enhanced accumulation of liposomes occurred in mice subjected to TBI compared to controls and accumulation was greater in the injured vs. the contralateral side of the brain (11). The aforementioned strategies for BBB opening may be invasive, not specific and lack precise control over the site and timing of BBB opening, which may limit their clinical translation. One novel approach based on a combination of stem cell delivery, heat-inducible gene expression and mild heating with high-intensity focused ultrasound (HIFU) under MRI guidance has been proposed to remotely permeabilize the BBB (Figure 2B) (59). The permeabilization of the BBB was controlled with and limited to where selected pro-inflammatory factors such as tumor necrosis factor alpha (TNFα) were secreted. In particular, mesenchymal stem cells (MSC) transduced with firefly luciferase (F-Luc) and tumor necrosis factor alpha (TNFα) or green fluorescence protein (GFP) driven by heat-inducible HSP70 promoter [MSCs-HSP70(F-Luc-2A-TNFα); MSCs-HSP70(F-Luc-2A-GFP)] were intracranially implanted into the right frontal lobe of athymic nude rats. Three days after implantation, HIFU was applied under MRI guidance and temperature was locally raised (Figure 2B, top and middle rows, firsts from left) in order to activate the heat-inducible promoter. Rats were then imaged for bioluminescence (BLI) after being injected i.p. with D-luciferin. Luciferase activity was detected in rat brains implanted with MSCs-HSP70(F-Luc-2A-TNFα) or MSCs-HSP70(F-Luc-2A-GFP) treated by HIFU, while rats implanted with MSCs-HSP70(F-Luc-2A-TNFα) without HIFU treatment showed background luciferase activity (Figure 2B, top row, second, third and fourth from left), indicating gene expression induced by HIFU. Contrast-enhanced T1-weighted MRI images were also acquired in order to verify the change of BBB permeability in the treated site. Enhancement was observed in the targeted regions of the rat brain implanted with MSCs-HSP70(F-Luc-2A-TNFα) construct and treated with HIFU. In contrast, rats implanted with MSCs-HSP70(F-Luc-2A-TNFα) without HIFU treatment and rats implanted with MSCs-HSP70(F-Luc-2A-GFP) with HIFU treatment did not demonstrate significant contrast enhancement on T1-weighted images (Figure 2B, middle row, second, third and fourth from left). Quantitative analysis of the T1-weighted images revealed a threefold contrast-enhancement in the target regions compared to the controls (Figure 2B, bottom row, left). Further, a mixture of fluorescent PLGA NP with different sizes (100 and 300 nm diameter) corresponding to different fluorescent labels were administered intravenously into the rats after HIFU-induced BBB opening (Figure 2B, bottom row, right). Both red fluorescence and green fluorescence were observed in the brain tissues, indicating that both 100 and 300 nm PLGA NP

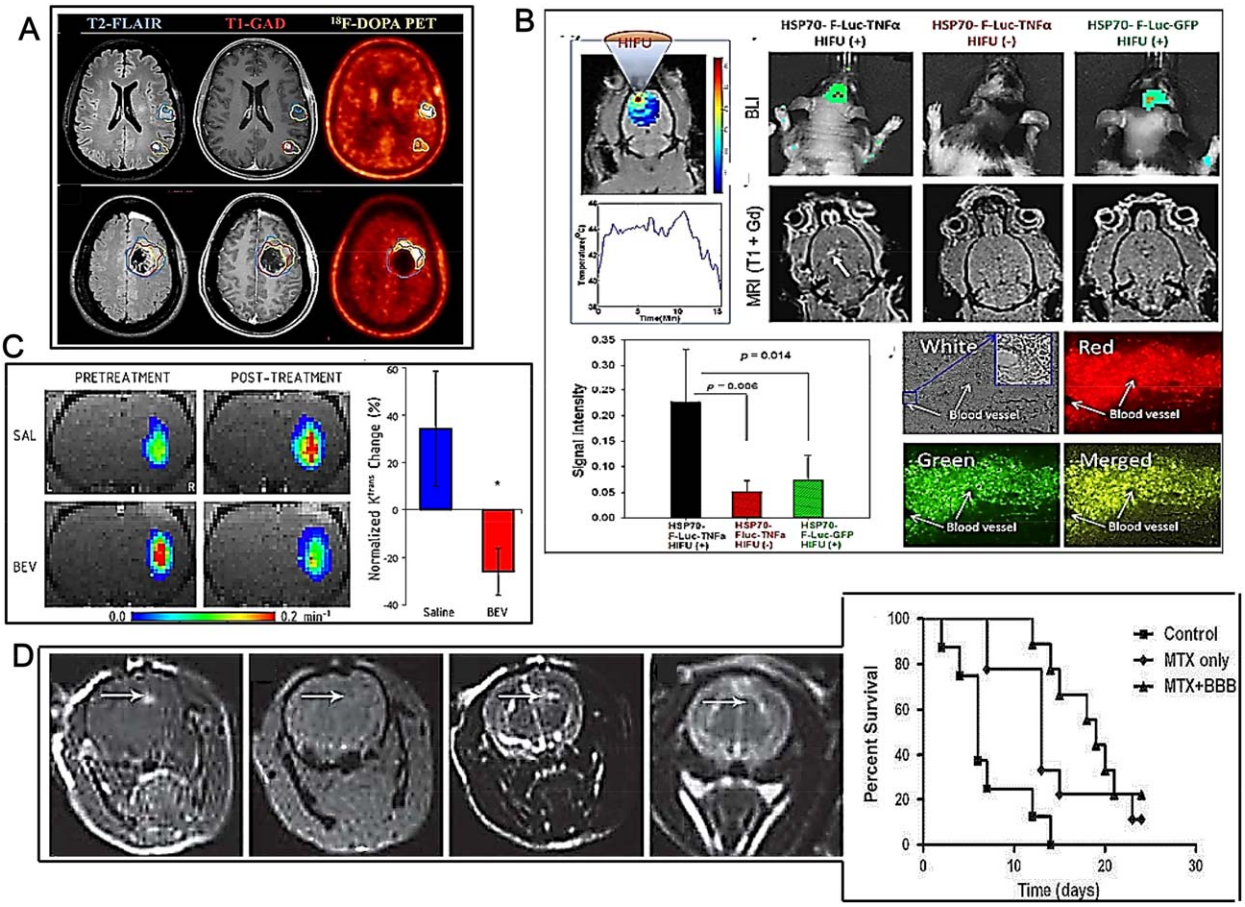


**Figure 2.** Advances in permeabilization-enhanced brain delivery. **A.** Different imaging modalities visualize tumors residing behind an intact BBB. First row: patient exhibiting multifocal GB. Second row: another patient 3 weeks post-surgical resection exhibits obvious tumor that was missed during surgery (after Ref. 7 with permission). **B.** MRI-guided HIFU activation of TNFα production by MSCs to permeabilize BBB. MSCs-HSP70(F-Luc-2A-TNFα) or MSCs-HSP70(F-Luc-2A-GFP) were stereotactically implanted into the brains of athymic nude rats. Temperature map of the injection area when heated by HIFU under guidance of MRI to induce TNFα expression 3 days after cell implantation (first and second rows, first images from left). First row, second, third and fourth images from left: the luciferase expression by bioluminescence after luciferin injection 1 day after HIFU induction. Second row, second, third and fourth images from left: T1-weighted MRI images after intravenous injection of the MRI contrast agent two days after HIFU induction. Third row, first image from left: quantification of the signal intensity of T1-enhanced contrast in the region of interest in the brains of rats after systemic injection of MR contrast agent. Second image from left (in four displays): BBB opening for NP penetration. Red (ii): red fluorescence-labeled PLGA NP. Green (iii): green fluorescence labeled PLGA NP. The brain blood vessels were indicated by white arrows (i, ii, iii, iv) (after Ref. 59 with permission). **C.** Bevacizumab may decrease tumor vessel permeability. Left: representative Ktrans maps of A549 intracerebral xenografts before and after saline (first row; SAL) or bevacizumab (second row; BEV). Right: normalized change in Ktrans in the saline control and bevacizumab-treated animals. $*P < 0.05$ vs. saline control group (after Ref. 43 with permission). **D.** BBB permeabilization in naive rats by EA–HSA. EA–HSA at 20 $\mu$g/rat was infused into the rats brains by CED. Left panel: T1-weighted MR images acquired 30 minutes after treatment (i, first from left). Gradient echo MR image acquired immediately post treatment (ii, second from left). T2-weighted images acquired immediately after treatment (iii, third from left) and T2-weighted images acquired 7 days after treatment (iv, fourth from left). The images reflect BBB opening depicted as bright enhancement on the T1-weighted MR images (i, indicated by arrows), no procedure-related hemorrhages (ii) neither tissue toxicity 7 days after treatment (iv). The images acquired immediately post CED (iii) show enhancement in the treated region induced by the convective distribution of the infusate. Right panel: Kaplan-Meier curves of the three treatment groups. Long-rank test resulted in $P < 0.001$ between all groups. BBB, blood brain barrier opening; MTX, methotrexate. (after Ref. 16 with permission).

successfully crossed the BBB after HIFU-induced TNFα production by MSC and penetrated to the brain tissues. No NP accumulation was found in brains from control groups. Hence, the permeabilization-enhanced brain delivery was hypothesized to be controlled with and limited to where selected pro-inflammatory factors such as TNFα are being secreted which may be in the vicinity of disease foci. Albeit this therapeutic platform is proposed as a non-invasive way for BBB opening with spatiotemporal precision, it may not be readily translated to patients, requiring complex conditions not easily achievable in the clinical setting (59).

A window period between anti-VEGF antibody bevacizumab and cytotoxic agents may enhance drug delivery to tumor tissue through bevacizumab-induced vascular normalization. In particular, administering bevacizumab 1 day earlier slightly improved the tumor-targeting of etoposide and cisplatin in patients with brain metastases of breast cancer (33). The results of this study were yet limited by the lack of a control arm. Opposite results were further obtained by Pishko and coworkers who studied the effect of bevacizumab on MRI biomarkers of brain tumor vascular characteristics in a rat model of human lung cancer brain metastasis (43). Ktrans as a measure of vascular permeability was determined using dynamic contrast-enhanced MRI. Compared to controls, bevacizumab treatment slowed the rate of tumor growth and blocked the increase in edema, but did not alter tumor blood volume. Bevacizumab specifically reduced Ktrans to $^{14}$C-aminoisobutyric acid in the tumor (AIB, Figure 2C). The results suggested that bevacizumab partially restored the normal low permeability characteristics of the BBB (43). Hence, the increased therapeutic effect observed by Lu and coworkers on brain metastases of breast cancer (33) may be linked to reduced tumor angiogenesis caused by bevacizumab rather than increased permeability to etoposide and cisplatin. Further studies are required in order to determine the major effects of bevacizumab in combination to chemotherapeutics over BBB opening.

Various human serum albumin (HSA) analogs have been synthesized and screened for BBB disruption efficacy. The candidate analogs were delivered into rat brains by CED and screened for maximal BBB disruption and minimal brain toxicity. Ethylamine-HAS was eventually selected as a possible BBB-opening agent and immunocytochemical studies suggested that BBB disruption by ethylamine-HSA could be linked to alterations in occludin expression. An efficacy study in rats bearing intracranial HGG showed that CED of EA-HSA in parallel to systemic administration of methotrexate caused a slightly prolonged animal survival in comparison to controls (Figure 2D) (16). Ultrasound contrast agents (UCA) rely on the high degree of echogenicity of specific, commercially available, gas-filled microbubbles as compared to the soft tissues of the body. UCA enhance the backscatter of the ultrasound waves to produce a sonogram with high contrast and have been explored as well to reversibly open the BBB (13). It has been reported that low-frequency ultrasound with UCA could temporarily and reversibly open the BBB in HGG rodent models and improve the penetration of the BBB by different drugs. A length of half a minute ultrasound was appropriate for opening BBB with no damage to brain tissue and facilitated drugs injected just before, entering the brain (13). In some cases, because of their relatively large size, the lifetime of microbubbles in the circulation system may be short (in the order of minutes) thus impairing penetration of the drug through the endothelial gap to enter the tumor and when microbubbles collapse is fast (a phenomenon termed "inertial cavitation") a shock wave causing intracerebral hemorrhaging leading to acute and chronic brain injury may be produced (18). The issue of microbubbles instability has been addressed after observing that in an acoustic field, droplets of particular liquefied gases such as perfluoropentane may be able to vaporize in a few cycles of exposure, a phenomenon termed "acoustic droplet vaporization" (63). The perfluoropentane microbubbles formed by acoustic droplet vaporization display enhanced stability thus allowing to enhance the shear stress to endothelial cells along the microvessels and increasing the number of BBB disrupted sites. A more homogenous drug distribution may thus be achieved by acoustic droplet vaporization without the elevated risks of tissue injury caused by inertial cavitation (18). It has been suggested that, likewise perfluoropentane, the excitation of BCNU bubbles by resonance frequency-matched FUS may result in a predominantly stable cavitation with little shock wave thus reducing the potential hazards during the BBB opening process. In tumor-bearing animals, BCNU bubbles combined with FUS allowed some control of tumor progression and improvement of survival (18). Dynamic contrast-enhanced MRI (DCE-MRI) has been used to characterize the FUS-induced permeability changes in a rat HGG model at different times after tumor implantation. 9L gliosarcoma cells were implanted in both hemispheres in male rats and at increasing times after implantation, FUS-induced BTB disruption using UCA microbubbles was performed in one tumor in each animal. Before FUS, liposomal doxorubicin had been administered, a chemotherapy agent that might be active against HGG. With FUS-induced BTB disruption, the doxorubicin concentrations in tumor tissues were increased to a limited extent (two-fold) with respect to control tumors. The FUS-induced increases in tumor drug delivery were relatively consistent over time suggesting that even late-stage tumors may benefit from FUS-induced drug enhancement (3).

The endothelial cell receptor molecule Roundabout 4 (ROBO4) is endogenously expressed in human brain microvascular endothelial cells and is upregulated in a BTB model of HGG- co-cultured endothelial cells. Knockdown of ROBO4 by short hairpin RNA (SHROBO4) led to decreased transendothelial electric resistance values, increased the BTB permeability and downregulated the expression of the endothelial cells tight junction proteins ZO-1, occludin, and claudin-5. Albeit the significance of these data is limited, being obtained in an *in vitro* co-culture system only, they suggest that knockdown of ROBO4 may increase the BTB permeability by reducing the expression of endothelial cells tight junction proteins (12). Bradykinin is a physiologically and pharmacologically active peptide of the kinin group of proteins, dilating blood vessels via the release of prostacyclin, nitric oxide and endothelium-derived hyperpolarizing factor. A bradykinin analog, retro-inverso bradykinin (RI-BK) which is characterized by resistance to proteolysis and binding activity with the bradykinin type 2 receptor has been developed (57). After systemic administration, RI-BK could induce a change in zonula occluden-1 and depolymerization of F-actin to selectively open the BTB. RI-BK increased the accumulation of drug-loaded NP in the HGG but not in normal brain, slightly improving their therapeutic efficacy (57). A laser-assisted hyperthemic method to induce temporary disruption of the peritumoral BBB has been evaluated in fourteen patients with recurrent GB (32). MRI-guided laser interstitial thermal therapy was applied to achieve both tumor cytoreduction and disruption of the peritumoral BBB. In all patients, Ktrans levels peaked immediately post laser ablation followed by a gradual decline over the following 4 weeks. Serum concentrations of brain-specific enolase, also known as neuron-specific enolase, increased shortly after laser ablation and peaked in 1–3 weeks before decreasing to baseline by 6 weeks. Hence, disruption of the peritumoral BBB was induced by hyperthermia with a peak of high permeability occurring within 1–2 weeks after laser ablation and resolving by 4–6 weeks, thus providing a therapeutic window of opportunity

during which delivery of BBB-impermeant therapeutic agents may be improved (32).

## POLYMERIC DEPOTS

Polymeric depots allowing gradual release of drugs in order to achieve high local concentrations while limiting systemic toxicities have been explored with limited success (54). Polymerically delivered carmustine (BCNU) wafers placed on the surface of the tumor-resection cavity and used to provide immediate chemotherapy to residual tumor cells during the standard delay between surgery and chemo/radiotherapy represent a controversial topic among neurosurgeons. The rationale, biochemistry, PK and research history (including toxicity profile) of this modality have been recently reviewed (54). In particular, a recent meta-analysis focused on whether carmustine wafer treatment could significantly benefit the survival of patients with newly diagnosed HGG. Six studies including two randomized controlled trials (RCT) and four cohort studies were considered. Carmustine wafers showed a limited advantage when pooling all the included studies. However, the two RCT did not show a statistical increase in survival in the group with carmustine wafer compared to the group without it, while the cohort studies demonstrated a significant survival increase. The presence of an internal randomized control arm in clinical trials (as in any other scientific investigation) is fundamental in order to obtain reliable results (20) and the results of the RCT deserve major consideration. BCNU wafer implantation as monochemotherapy (with RT) in newly diagnosed HGG has been investigated in two phase III studies that reported limited increases in median overall survival. A number of studies have investigated the tumoricidal synergies of experimental new drugs with BCNU wafers in newly diagnosed or recurrent HGG which have shown limited improvements in efficacy of treatments (58). Overall, the therapeutic efficacy of treatment with carmustine wafers in HGG patients is limited or null.

A polyethylene glycol dimethacrylate (PEG-DMA) injectable hydrogel that photopolymerizes *in situ* and may thus fit the borders of the resected zone thus providing sustained, local drug delivery has been investigated in order to improve local delivery of TMZ (Figure 3A) (19). The hydrogel photopolymerized rapidly and presented a viscous modulus (approximately 10 kPa). The TMZ release kinetics presented two phases: a linear burst release of 45% of TMZ during the first 24 h, followed by a logarithmic release of 20% over the first week. The *in vivo* tolerability study showed that the unloaded hydrogel did not induce apoptosis in mice brains nor increased microglial activation. *In vivo*, the anti-tumor efficacy of TMZ-hydrogel was evaluated on xenograft U87 tumor-bearing nude mice. The tumor weight of mice treated with the photopolymerized TMZ hydrogel decreased compared with all control groups and higher apoptosis was observed located at the center of the tumor (19). No data on overall survival of animals were reported.

Poly(epsilon-caprolactone)-random-poly(D,L-lactide)-block-poly (ethyleneglycol)-block-poly(epsilon-caprolactone)-randompoly(D,L-lactide) (PLEC) polymeric depots have been used to administer SN-38 directly to U87 orthotopic tumors. SN-38 released from depots reduced tumor growth, where the extent of the reduction depended on the doses and number of depot injections. Tumor reduction of SN-38 from depots was threefold higher in animals which received double injections of depots at high dose compared to single injection. Hematoxylin and eosin (H/E) staining of tumor sections showed that the area of tumor cell death/survival of the former group was twofold higher than those of the latter group. Fluorescence imaging based on the self-fluorescent property of SN-38 was used to evaluate the intratumoral distribution of this drug compared to histological results. The linear correlation between fluorescence intensity and the amount of SN-38 allowed quantitative determination of SN-38 in tumor tissues. A direct correlation between the amount of SN-38 in tumor sections and cancer cell death was found and a 3D reconstruction representing the distribution of SN-38 in tumors was reported (53). An electrospinning technique and biodegradable PLGA nanofibrous membranes facilitating a sustained release of BCNU, irinotecan and cisplatin have been developed (49). Elution coupled to high-performance liquid chromatography (HPLC) was employed to characterize the *in vitro* and *in vivo* release of pharmaceuticals from the membranes. The biodegradable, nanofibrous membranes released high concentrations of BCNU, irinotecan and cisplatin for more than 8 weeks in the cerebral cavity of rats where progressive atrophy of the brain tissues was observed. The scalp wound and the brain tissue were relatively clear and no infection (no exudate, pus, or granulation formation) was observed (Figure 3B) (49).The normolipidemic drug fenofibrate (FF) has been shown to exert some effects against tumors of neuroectodermal origin including HGG. HPLC has been used to elucidate the intracellular, tissue and body fluid distribution of FF and FA after oral administration of the drug to mice bearing intracranial HGG. Following the oral treatment, FF was quickly cleaved to FA by blood esterases and FA was detected in the blood, urine, liver, kidney, spleen and lungs. Small amounts of FA were also detected in the brains of two out of six mice, but not in the brain tumor tissue. The lack of FF and FA in the intracranial tumors prompted to develop *in vitro* biodegradable PLGA polymer wafers containing FF. The fabrication consisted of two-layered porous biodegradable PLGA films where FF was incorporated into the bottom layer and sealed with a second PLGA layer without drug. This depot can then be inserted into the brain cavity following resection of the brain tumor (Figure 3C). HPLC-based analysis demonstrated a slow and constant diffusion of FF from the wafer and the released FF abolished clonogenic growth of HGG cells. On the intracellular level, FF and FA were both present in the cytosolic fraction while FF, but not FA, was detected in the cell membrane fraction (23). Disulfiram (DSF), which is an antialcoholic drug, has been suggested to have a copper-dependent anticancer effect against HGG. Different manufacturing techniques of DSF-loaded biodegradable wafers including compression and solvent casting have been compared with respect to DSF delivery (61). Neither technique had an adverse effect on the stability of the DSF within the wafers but release of the drug from the wafers was in part dependent on them (61). Treatments of brain tumor-associated edema with systemically delivered dexamethasone, the standard of care and cediranib, a novel anti-edema agent, may be associated with systemic toxicities in HGG patients (39). A tunable, reservoir-based drug delivery device has been developed in order to deliver dexamethasone and cediranib locally in the brain in an intracranial 9L gliosarcoma rat model (Figure 3D). Sustained releases of both dexamethasone and a solid dispersion of cediranib in polyvinylpyrrolidone (AZD/PVP) from these devices were achieved. Local delivery of dexamethasone and cediranib with this device was as effective as systemic delivery in alleviating edema, which was associated with some survival benefit. Local delivery of dexamethasone prevented dexamethasone-induced weight loss, an adverse effect seen in animals treated with systemic dexamethasone.

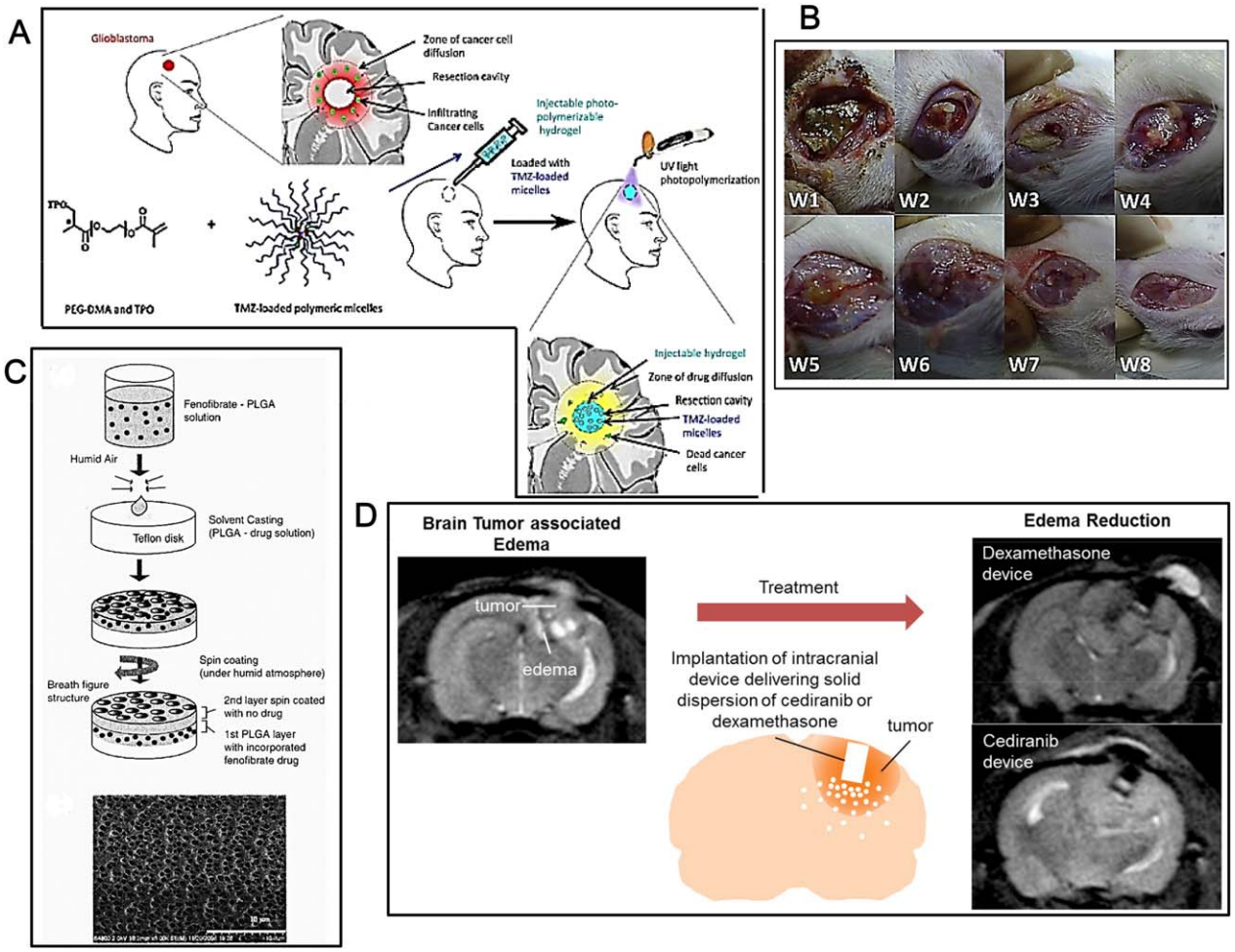


**Figure 3.** Advances in polymeric depots. **A.** Development of an injectable hydrogel loaded with TMZ-loaded polymeric micelles. From top left clockwise: the new injectable delivery system (i) fits the resection cavity, (ii) can be easily and quickly polymerized *in situ* via a commercial device, (iii) localizes and sustainably releases anti-cancer drugs directly to the invaded parenchyma where apoptosis of HGG cells may be increased (iv) (after Ref. 19 with permission). **B.** Gross wound conditions after implantation of PLGA membrane releasing BCNU, irinotecan and cisplatin. The number at the bottom left corner of each image indicates the number of weeks that have passed after the implantation of the PLGA nanofibrous membrane. The biodegradable PLGA nanofibrous membrane degraded with time and almost disappeared by week 8 (after Ref. 49 with permission). **C.** Schematic description of the preparation of PLGA wafers containing FF. From top to bottom: (i) FF was first dissolved in methylene chloride followed by addition of the PLGA polymer. (ii) An appropriate volume of the solution containing PLGA and the drug was solvent-cast onto a Teflon disk under constant humidity, thus allowing slow evaporation of solvent and (iii) production of a so-called "breath" pattern of regular pores in the polymer film enhancing its drug delivery properties. (iv) To coat a second layer, PLGA solution in methylene chloride was spin-coated over the first layer, again under humid atmosphere to create pores on the top layer. (v) A scanning electron microscope (SEM) photomicrograph of a porous membrane fabricated as above is shown at bottom (after Ref. 23 with permission). **D.** A tunable, reservoir-based drug delivery device (ii) permits delivering dexamethasone and cediranib locally in the brain in an intracranial 9L gliosarcoma rat model (i, iii). The device is comprised of a reservoir of solid drug formulation and a cap with orifices through which the drug is released (ii) (after Ref. 39 with permission).

Local deliveries of dexamethasone and cediranib via these devices may thus allow using lower doses as compared to systemic administration, achieving similar efficacy without the corresponding side effects (39).

## OMMAYA RESERVOIRS

Ommaya reservoirs are catheter systems usually placed in one lateral ventricle attached to a reservoir implanted under the scalp, employed in most (four out of five) cases to treat HGG by intrathecal chemotherapy (Figure 4A). They were originally invented in 1963 by Ayub K. Ommaya, a Pakistani neurosurgeon. Ommaya reservoirs provide fast access and reliable drug delivery to cerebral spinal fluid. Complications of Ommaya reservoir placement and its use mainly consist of early infectious causes (35). Two rare cases of encephaloclastic cyst with intraventricular topotecan use have been reported. This pathogenesis may result from retrograde flow of intraventricular chemotherapy into the brain parenchyma and subsequent development of a local chemical encephalopathy. The

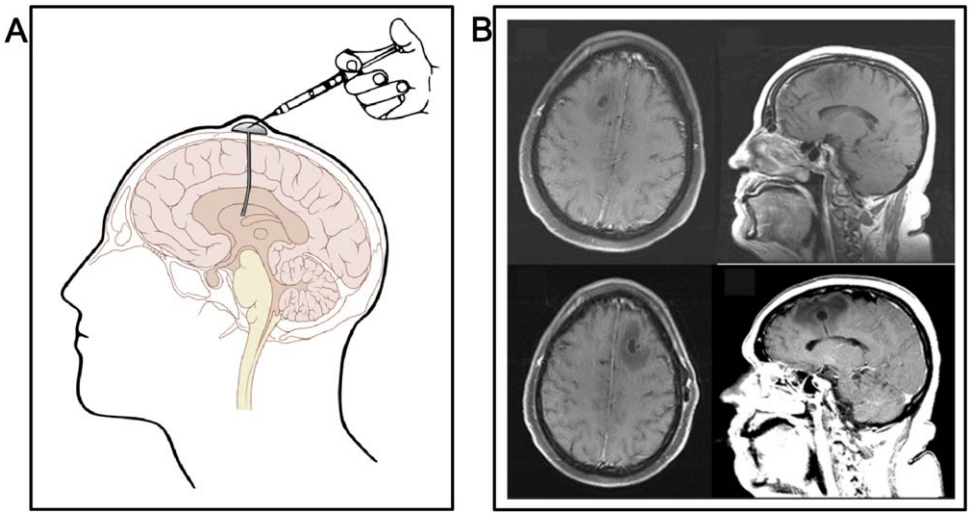


**Figure 4.** Advances in Ommaya reservoirs. **A.** Schematic representation of an implanted Ommaya reservoir. After an artwork by Patrick J. Lynch, with permission. **B.** MRI of the brain of a 65-year old woman with an implanted Ommaya reservoir for intraventricular therapy with topotecan, showing a cystic dilatation of the brain parenchyma with vasogenic edema surrounding the catheter connecting to the reservoir dome and delivering the drug to the intraventricular space (Figure 4B, first row). After removing the Ommaya reservoir because of neurological symptoms including left-sided weakness, confusion and headaches, the neurosurgeons found no evidence of tumoral infiltration or infection and another Ommaya reservoir was placed in the contralateral side in order to avoid discontinuation of therapy. After 7 treatments, the patient displayed yet similar neurological symptoms and radiological findings and the treatment had to be halted (Figure 4B, second row) (after Ref. 35 with permission).

two patients presented with metastatic cancers complicated by leptomeningeal disease. Ommaya reservoirs were placed in both cases and patients were treated with intraventricular topotecan twice weekly. After one dozen of intraventricular treatments, both patients developed confusion, seizures and headaches. MRI of the brain demonstrated cystic dilatation of the brain parenchyma around the catheter that connects to the reservoir dome and delivers the drug to the intraventricular space (Figure 4B). The catheter was surrounded by vasogenic edema. Catheters were removed and analyzed and were found to be intact. Cerebrospinal fluid analyses showed no evidence of infection or malignancy. Intraventricular topotecan was discontinued and both patients demonstrated sustained clinical and radiological response. Albeit complications of intraventricular delivery of drugs to HGG patients by Ommaya reservoirs may thus be managed (35), the data confirm that addition of intraventricular chemotherapy does not lead to survival benefit or improved response to neurooncologic patients, partially linked to inability to achieve clinically relevant tissue penetration (9).

## FURTHER DELIVERY MODES

### Intra-arterial

Intra-arterial (IA) drug delivery is a physiologically appealing strategy as drugs may be widely distributed throughout the tumor capillary network and high regional tissue concentrations could be achieved with relatively low doses (29). Albeit IA drug administration for HGG has been explored since the 1950s as an attempt to improve drug delivery, the question whether IA administration is safe and more effective compared to other delivery modalities remains open with a number of critical oversights (30). In particular, IA-delivered drugs have often been found unable to penetrate the BBB and their PK still is poorly understood. Despite those limits, clinical interest in IA drugs for the treatment of HGG persists, linked to improved drug selections and formulations as well as novel methodologies allowing better definition of the HGG morphology and lower treatment-related neurological injury (29). These studies may take advantage of a recently developed mouse model of IA drug delivery accessing the internal carotid artery to treat ipsilateral implanted HGG tumors (30, 42).

### Intranasal

As unfortunately cocaine users demonstrate, the intranasal administration may anticipate a certain level of brain delivery as the nasal route possesses direct access to the brain. Experimental drugs administered for HGG treatment via the intranasal route include a polymeric NP formulation of carboplatin (1) and perillyl alcohol (POH) (14). The latter is a naturally occurring dietary monoterpene isolated from the essential oils of lavender, peppermint and other plants. Medical interest in this compound was generated by some research findings suggesting that POH was able to partially inhibit the growth of tumor cells in cell culture and exert cancer preventive and therapeutic activity in some animal tumor models. Attempts to treat cancer patients with oral POH had to be yet soon abandoned because of elevated toxicity. The intranasal POH delivery has been clinically explored in two Brazilian trials in order to circumvent the toxic limitations of oral administration. Patients with recurrent HGG were given comparatively small doses of POH via simple inhalation through the nose. This type of long-term, daily chemotherapy was well tolerated but its effects in therapy of patients with HGG were negligible (14). During the end-of-life (EOL) phase of

HGG patients, a rapid deterioration in neurological functioning may interfere with the oral intake of antiepileptic drugs (AED). The feasibility of intranasal AED treatment in an out-of-hospital setting has been investigated (31). In six patients receiving treatment with intranasal midazolam, partial seizure control was achieved and none of the patients needed to be transferred to the hospital because of recurrent seizures. Although studies with higher numbers of patients are certainly required, it might be feasible to treat seizures with intranasal benzodiazepines in the EOL phase of HGG patients, as it may make caregivers able to manage seizures at home (31).

### Stereotactic Injections and Osmotic Pumps

Intratumoral hypoxia is thought to contribute to tumorigenesis and angiogenesis in HGG. Because hypoxia-inducible factor 1 alpha (HIF-1alpha) is a major mediator of hypoxia-regulated cellular proliferation, inhibition of this transcription factor may reduce HGG growth. Using an orthotopic mouse model with U87-LucNeo cells, RNA interference was applied in order to knock down HIF-1alpha *in vivo*. The small interfering RNA (siRNA) was packaged using a novel multifunctional surfactant, 1-(aminoethyl) iminobis[N-(oleicylcysteinylhistinyl-1-aminoethyl)propionamide] (EHCO), a nucleic acid carrier that facilitates cellular uptake and intracellular release of siRNA. Stereotactic injection by a Hamilton syringe was used to deliver the siRNA package locally through a guide-screw system and delivery/uptake was verified by imaging of fluorescently labeled siRNA. Alternatively, osmotic pumps were used for sustained siRNA delivery. Mice receiving siRNA injection targeting HIF-1alpha displayed a lower tumor volume after 50 days of treatment than the controls and levels of the HIF-1 transcriptional targets vascular endothelial growth factor (VEGF), glucose transporter 1 (GLUT-1), c-MET and carbonic anhydrase-IX and markers for cell growth (MIB-1 and microvascular density) were lower as well. Addition of polyethylene glycol to the carrier EHCO increased the efficacy of drug delivery and even survival (22).

### Conjugation

The anticancer drug MTX has poor permeability across the BBB making it unsuitable for brain tumor application. Possible improvements in brain availability and scope of application were investigated by reversible conjugation with lysine by an amide linkage in order to exploit the endogenous transport system of lysine at BBB (47). The structure of prodrug was confirmed by mass spectrometry and stability and metabolic studies suggested that the conjugate was stable at physiological pH and could release MTX slowly to the brain. *In vivo* biodistribution studies showed that the conjugate prodrug remarkably increased the level of MTX 5.8 fold in brain when compared with PK parameters of unconjugated MTX (47).

### Exosomes

Whether brain endothelial cell-derived exosomes can deliver anticancer drugs across the BBB for the treatment of brain cancer has been investigated in a zebrafish (Danio rerio) model. Exosomes derived from brain endothelial cells expressed detectable CD63 tetraspanins transmembrane proteins, cell-surface proteins regulating cell activation, growth and motility. Exosomes increased the uptake of fluorescent markers via receptor-mediated endocytosis and the cytotoxicity of anticancer drugs toward cancer cells. Images of the zebrafish showed exosome-delivered anticancer drugs crossing the BBB and entering the brain. In a brain cancer model, the delivered anticancer drugs decreased the fluorescent intensity of xenotransplanted cancer cells and tumor growth markers but no animal survival data were reported (60).

## PEDIATRIC SETTING

Brainstem tumors represent 10%–15% of pediatric CNS tumors and diffuse intrinsic pontine glioma (DIPG) is the most common among them (50). DIPG is almost invariably fatal and is the leading cause of brain tumor-related death in children. To date, RT is the only form of treatment that offers a transient benefit in DIPG. Multi-agent neoadjuvant chemotherapy, concurrent chemotherapy with RT and adjuvant chemotherapy have not provided any survival advantage so far. To overcome the restrictive ability of the intact BBB in DIPG, several alternative drug delivery strategies alone or in combination with RT have been proposed with minimal success. Likewise adults, BBB permeability is of major concern in DIPG patients and overcoming the barrier may ensure that drugs reach the tumor. The recent development of DIPG tumor models may help the identification and validation of therapeutic targets and small molecule inhibitors possibly useful for treatment (50). The IGF-1R/InsR inhibitor BMS-754807 might be one of them. Albeit this drug reduces tumor growth in a selected group of epithelial, hematopoietic and mesenchymal xenograft tumor models, its systemic administration did not prolong animal survival in DIPG animal models (25). PK studies demonstrated that the concentrations of BMS-754807 in DIPG tumor tissue were well below the identified $IC_{50}$, suggesting that inadequate drug delivery may limit its *in vivo* efficacy toward brain tumors, the umpteenth confirmation of the essential function of animal studies for development of effective drugs against HGG.

## CONCLUSIONS

If combating cancer is difficult, combating brain cancer is twice as difficult caused by the inability of most drugs to cross the BBB and BTB and achieve sufficient concentrations in the brain tumor tissues. Many novel experimental drugs active against body tumors fail in the treatment of brain tumors for this reason. In order to fix at least this part of the problem, several novel drug delivery techniques are being explored in both preclinical and clinical settings (21). Along this route, invasivity often clashes with efficacy: e.g. CED is probably the most effective intracranial drug delivery mode but involves a complex and invasive procedure requiring high-tech devices to date only available in a few experimental centers (2, 24). Similar and even higher concerns apply to techniques aiming to permeabilize the BBB, affected by limited spatiotemporal precision and high risks of iatrogenic disease. For those studies, the survival data related to the BBB opening procedure are rarely (while should be invariably) reported. On the other hand, less invasive techniques such as polymeric depots or intranasal administration may be affected by low delivery to the brain: e.g. drugs delivered through intranasal administration may be recruited mostly by the lungs rather than by the brain (56). Even for novel drugs crossing the BBB, it must be recalled that their systemic administration may cause important side effects: for

instance, radiosensitizers acting by stimulating the proliferation of quiescent GIC (eg, ATM inhibitors) may dangerously lead to hyperproliferation of mutated stem cells in normal epithelia (eg, in lungs and colon) when given systemically, thus increasing the risks of iatrogenic tumors. In other words, even if experimental drugs against HGG are found able to cross the BBB or procedures are developed for making them crossing the BBB, the long-term side effects of their systemic administration must be carefully evaluated in animals prior to passage to the Phase I clinics. The level of iatrogenic risk to which HGG patients can be ethically exposed is an important issue that lies beyond the scope of this article. Our opinion is that the intracranial delivery of drugs to brain tumor tissues by effective loco-regional modes (eg, by developing simpler and safer CED or Ommaya devices), might be the route of choice, rather than improved passage through the BBB, in order to achieve the highest efficacy/safety ratio of drugs against HGG.

## ACKNOWLEDGMENTS

This work was partially supported by Compagnia San Paolo, Turin, Italy (grant no. 2010.1944 and Project "Terapie innovative per il glioblastoma").

## REFERENCES

1. Alex AT, Joseph A, Shavi G, Rao JV, Udupa N (2015) Development and evaluation of carboplatin-loaded PCL nanoparticles for intranasal delivery. *Drug Deliv* 1–10 [Epub ahead of print].
2. Arshad A, Yang B, Bienemann AS, Barua NU, Wyatt MJ, Woolley M *et al* (2015) Convection-enhanced delivery of carboplatin PLGA nanoparticles for the treatment of glioblastoma. *PLoS One* **10**: e0132266.
3. Aryal M, Park J, Vykhodtseva N, Zhang YZ, McDannold N (2015) Enhancement in blood-tumor barrier permeability and delivery of liposomal doxorubicin using focused ultrasound and microbubbles: evaluation during tumor progression in a rat glioma model. *Phys Med Biol* **60**:2511–2527.
4. Azad TD, Pan J, Connolly ID, Remington A, Wilson CM, Grant GA (2015) Therapeutic strategies to improve drug delivery across the blood-brain barrier. *Neurosurg Focus* **38**:E9.
5. Bao S, Wu Q, McLendon RE, Hao Y, Shi Q, Hjelmeland AB *et al* (2006) Glioma stem cells promote radioresistance by preferential activation of the DNA damage response. *Nature* **444**:756–760.
6. Beccaria K, Canney M, Goldwirt L, Fernandez C, Piquet J, Perier MC *et al* (2016) Ultrasound-induced opening of the blood-brain barrier to enhance temozolomide and irinotecan delivery: an experimental study in rabbits. *J Neurosurg* **124**:1602–1610.
7. Becker CM, Oberoi RK, McFarren SJ, Muldoon DM, Pafundi DH, Pokorny JL *et al* (2015) Decreased affinity for efflux transporters increases brain penetrance and molecular targeting of a PI3K/mTOR inhibitor in a mouse model of glioblastoma. *Neuro Oncol* **17**: 1210–1219.
8. Bhowmik A, Khan R, Ghosh MK (2015) Blood brain barrier: a challenge for effectual therapy of brain tumors. *Biomed Res Int* **2015**: 320941.
9. Boogerd W, van den Bent MJ, Koehler PJ, Heimans JJ, van der Sande JJ, Aaronson NK *et al* (2004) The relevance of intraventricular chemotherapy for leptomeningeal metastasis in breast cancer: a randomised study. *Eur J Cancer* **40**:2726–2733.
10. Bouras A, Kaluzova M, Hadjipanayis CG (2015) Radiosensitivity enhancement of radioresistant glioblastoma by epidermal growth factor receptor antibody-conjugated iron-oxide nanoparticles. *J Neurooncol* **124**:13–22.
11. Boyd BJ, Galle A, Daglas M, Rosenfeld JV, Medcalf R (2015) Traumatic brain injury opens blood-brain barrier to stealth liposomes via an enhanced permeability and retention (EPR)-like effect. *J Drug Target* **23**:847–853.
12. Cai H, Liu W, Xue Y, Shang X, Liu J, Li Z *et al* (2015) Roundabout 4 regulates blood-tumor barrier permeability through the modulation of ZO-1, occludin, and claudin-5 expression. *J Neuropathol Exp Neurol* **74**:25–37.
13. Chen LJ, Lu CT, Zhao YZ, Du LN, Jin YG (2015) Ultrasonic microbubbles for glioma-targeted drug delivery. *Yao Xue Xue Bao* **50**:99–103.
14. Chen TC, Fonseca CO, Schonthal AH (2015) Preclinical development and clinical use of perillyl alcohol for chemoprevention and cancer therapy. *Am J Cancer Res* **5**:1580–1593.
15. Chittiboina P, Heiss JD, Lonser RR (2015) Accuracy of direct magnetic resonance imaging-guided placement of drug infusion cannulae. *J Neurosurg* **122**:1173–1179.
16. Cooper I, Last D, Guez D, Sharabi S, Elhaik Goldman S, Lubitz I *et al* (2015) Combined local blood-brain barrier opening and systemic methotrexate for the treatment of brain tumors. *J Cereb Blood Flow Metab* **35**:967–976.
17. Danhier F, Messaoudi K, Lemaire L, Benoit JP, Lagarce F (2015) Combined anti-galectin-1 and anti-EGFR siRNA-loaded chitosan-lipid nanocapsules decrease temozolomide resistance in glioblastoma: in vivo evaluation. *Int J Pharm* **481**:154–161.
18. Fan CH, Ting CY, Chang YC, Wei KC, Liu HL, Yeh CK (2015) Drug-loaded bubbles with matched focused ultrasound excitation for concurrent blood-brain barrier opening and brain-tumor drug delivery. *Acta Biomater* **15**:89–101.
19. Fourniols T, Randolph LD, Staub A, Vanvarenberg K, Leprince JG, Preat V *et al* (2015) Temozolomide-loaded photopolymerizable PEG-DMA-based hydrogel for the treatment of glioblastoma. *J Control Release* **210**:95–104.
20. Frosina G (2015) Limited advances in therapy of glioblastoma trigger re-consideration of research policy. *Crit Rev Oncol Hematol* **96**:257–261.
21. Frosina G (2016) Nanoparticle-mediated drug delivery to high-grade gliomas. *Nanomedicine* **12**:1083–1093.
22. Gillespie DL, Aguirre MT, Ravichandran S, Leishman LL, Berrondo C, Gamboa JT *et al* (2015) RNA interference targeting hypoxia-inducible factor 1alpha via a novel multifunctional surfactant attenuates glioma growth in an intracranial mouse model. *J Neurosurg* **122**:331–341.
23. Grabacka M, Waligorski P, Zapata A, Blake DA, Wyczechowska D, Wilk A *et al* (2015) Fenofibrate subcellular distribution as a rationale for the intracranial delivery through biodegradable carrier. *J Physiol Pharmacol* **66**:233–247.
24. Halle B, Marcusson EG, Aaberg-Jessen C, Jensen SS, Meyer M, Schulz MK *et al* (2016) Convection-enhanced delivery of an anti-miR is well-tolerated, preserves anti-miR stability and causes efficient target de-repression: a proof of concept. *J Neurooncol* **126**:47–55.
25. Halvorson KG, Barton KL, Schroeder K, Misuraca K, Hoeman C, Chung A *et al* (2015) A high-throughput in vitro drug screen in a genetically engineered mouse model of diffuse intrinsic pontine glioma identifies BMS-754807 as a promising therapeutic agent. *PLoS One* **10**:e0118926.
26. Healy AT, Vogelbaum MA (2015) Convection-enhanced drug delivery for gliomas. *Surg Neurol Int* **6**:S59–S67.
27. Hiramatsu R, Kawabata S, Tanaka H, Sakurai Y, Suzuki M, Ono K *et al* (2015) Tetrakis(p-carboranylthio-tetrafluorophenyl)chlorin (TPFC): application for photodynamic therapy and boron neutron capture therapy. *J Pharm Sci* **104**:962–970.
28. Jahangiri A, Chin AT, Flanigan PM, Chen R, Bankiewicz K, Aghi MK (2016) Convection-enhanced delivery in glioblastoma: a review of preclinical and clinical studies. *J Neurosurg* **1**:1–10.

29. Joshi S, Ellis JA, Ornstein E, Bruce JN (2015) Intraarterial drug delivery for glioblastoma mutiforme: Will the phoenix rise again? *J Neurooncol* **124**:333–343.
30. Kim M, Barone TA, Fedtsova N, Gleiberman A, Wilfong CD, Alosi JA *et al* (2015) A murine model of targeted infusion for intracranial tumors. *J Neurooncol* **126**:37–45.
31. Koekkoek JA, Postma TJ, Heimans JJ, Reijneveld JC, Taphoorn MJ (2016) Antiepileptic drug treatment in the end-of-life phase of glioma patients: a feasibility study. *Support Care Cancer* **24**:1633–1638.
32. Leuthardt EC, Duan C, Kim MJ, Campian JL, Kim AH, Miller-Thomas MM *et al* (2016) Hyperthermic laser ablation of recurrent glioblastoma leads to temporary disruption of the peritumoral blood brain barrier. *PLoS One* **11**:e0148613.
33. Lu YS, Chen TW, Lin CH, Yeh DC, Tseng LM, Wu PF *et al* (2015) Bevacizumab preconditioning followed by etoposide and cisplatin is highly effective in treating brain metastases of breast cancer progressing from whole-brain radiotherapy. *Clin Cancer Res* **21**: 1851–1858.
34. Mehta AI, Linninger A, Lesniak MS, Engelhard HH (2015) Current status of intratumoral therapy for glioblastoma. *J Neurooncol* **125**:1–7.
35. Mella DB, Kamiya-Matsuoka C, Liao B, Tummala S, de Groot J (2015) Recurrent encephaloclastic cyst induced by intraventricular topotecan. *J Neurol Sci* **349**:52–53.
36. Mendiburu-Elicabe M, Gil-Ranedo J (2015) Combination therapy of intraperitoneal rapamycin and convection- enhanced delivery of nanoliposomal CPT-11 in rodent orthotopic brain tumor xenografts. *Curr Cancer Drug Targets* **15**:352–362.
37. Morikawa A, Peereboom DM, Thorsheim HR, Samala R, Balyan R, Murphy CG *et al* (2015) Capecitabine and lapatinib uptake in surgically resected brain metastases from metastatic breast cancer patients: a prospective study. *Neuro Oncol* **17**:289–295.
38. Oberoi RK, Parrish KE, Sio TT, Mittapalli RK, Elmquist WF, Sarkaria JN (2016) Strategies to improve delivery of anticancer drugs across the blood-brain barrier to treat glioblastoma. *Neuro Oncol* **18**:27–36.
39. Ong Q, Hochberg FH, Cima MJ (2015) Depot delivery of dexamethasone and cediranib for the treatment of brain tumor associated edema in an intracranial rat glioma model. *J Control Release* **217**:183–190.
40. Parrish KE, Cen L, Murray J, Calligaris D, Kizilbash S, Mittapalli RK *et al* (2015) Efficacy of PARP inhibitor rucaparib in orthotopic glioblastoma xenografts is limited by ineffective drug penetration into the central nervous system. *Mol Cancer Ther* **14**:2735–2743.
41. Parrish KE, Sarkaria JN, Elmquist WF (2015) Improving drug delivery to primary and metastatic brain tumors: strategies to overcome the blood-brain barrier. *Clin Pharmacol Ther* **97**:336–346.
42. Peschillo S, Caporlingua A, Diana F, Caporlingua F, Delfini R (2015) New therapeutic strategies regarding endovascular treatment of glioblastoma, the role of the blood-brain barrier and new ways to bypass it. *J Neurointerv Surg* (in press).
43. Pishko GL, Muldoon LL, Pagel MA, Schwartz DL, Neuwelt EA (2015) Vascular endothelial growth factor blockade alters magnetic resonance imaging biomarkers of vascular function and decreases barrier permeability in a rat model of lung cancer brain metastasis. *Fluids Barriers CNS* **12**:5.
44. Pokorny JL, Calligaris D, Gupta SK, Lyekegbe DO Jr, Mueller D, Bakken KK *et al* (2015) The efficacy of the Wee1 inhibitor MK-1775 combined with temozolomide is limited by heterogeneous distribution across the blood-brain barrier in glioblastoma. *Clin Cancer Res* **21**: 1916–1924.
45. Ros M, Iorio AL, Lucchesi M, Stival A, Martino M, Sardi I (2015) The use of anthracyclines for therapy of CNS tumors. *Anticancer Agents Med Chem* **15**:721–727.
46. Singh I, Swami R, Jeengar MK, Khan W, Sistla R (2015) p-aminophenyl-alpha-D-mannopyranoside engineered lipidic nanoparticles for effective delivery of docetaxel to brain. *Chem Phys Lipids* **188**:1–9.
47. Singh VK, Subudhi BB (2015) Development and characterization of lysine-methotrexate conjugate for enhanced brain delivery. *Drug Deliv* 1–11 [Epub ahead of print].
48. Strohbehn G, Coman D, Han L, Ragheb RR, Fahmy TM, Huttner AJ *et al* (2015) Imaging the delivery of brain-penetrating PLGA nanoparticles in the brain using magnetic resonance. *J Neurooncol* **121**:441–449.
49. Tseng YY, Wang YC, Su CH, Yang TC, Chang TM, Kau YC *et al* (2015) Concurrent delivery of carmustine, irinotecan, and cisplatin to the cerebral cavity using biodegradable nanofibers: in vitro and in vivo studies. *Colloids Surf B Biointerfaces* **134**:254–261.
50. Vanan MI, Eisenstat DD (2015) DIPG in children—What can we learn from the past? *Front Oncol* **5**:237.
51. Vecchio D, Daga A, Carra E, Marubbi D, Baio G, Neumaier CE *et al* (2014) Predictability, efficacy and safety of radiosensitization of glioblastoma-initiating cells by the ATM inhibitor KU-60019. *Int J Cancer* **135**:479–491.
52. Vecchio D, Daga A, Carra E, Marubbi D, Raso A, Mascelli S *et al* (2015) Pharmacokinetics, pharmacodynamics and efficacy on pediatric tumors of the glioma radiosensitizer KU60019. *Int J Cancer* **136**: 1445–1457.
53. Vejjasilpa K, Nasongkla N, Manaspon C, Larbcharoensub N, Boongird A, Hongeng S *et al* (2015) Antitumor efficacy and intratumoral distribution of SN-38 from polymeric depots in brain tumor model. *Exp Biol Med (Maywood)* **240**:1640–1647.
54. Wait SD, Prabhu RS, Burri SH, Atkins TG, Asher AL (2015) Polymeric drug delivery for the treatment of glioblastoma. *Neuro Oncol* **17**(Suppl.2):ii9–ii23.
55. Watanabe M (2015) A novel in situ permeation system and its utility in cancer tissue ablation. *Int J Oncol* **47**:875–883.
56. Wheeler CJ, Felgner PL, Tsai YJ, Marshall J, Sukhu L, Doh SG *et al* (1996) A novel cationic lipid greatly enhances plasmid DNA delivery and expression in mouse lung. *Proc Natl Acad Sci U S A* **93**:11454–11459.
57. Xie Z, Shen Q, Xie C, Lu W, Peng C, Wei X *et al* (2015) Retro-inverso bradykinin opens the door of blood-brain tumor barrier for nanocarriers in glioma treatment. *Cancer Lett* **369**:144–151.
58. Xing WK, Shao C, Qi ZY, Yang C, Wang Z (2015) The role of gliadel wafers in the treatment of newly diagnosed GBM: a meta-analysis. *Drug Des Devel Ther* **9**:3341–3348.
59. Xiong X, Sun Y, Sattiraju A, Jung Y, Mintz A, Hayasaka S *et al* (2015) Remote spatiotemporally controlled and biologically selective permeabilization of blood-brain barrier. *J Control Release* **217**:113–120.
60. Yang T, Martin P, Fogarty B, Brown A, Schurman K, Phipps R *et al* (2015) Exosome delivered anticancer drugs across the blood-brain barrier for brain cancer therapy in danio rerio. *Pharm Res* **32**:2003–2014.
61. Zembko I, Ahmed I, Farooq A, Dail J, Tawari P, Wang W *et al* (2015) Development of disulfiram-loaded poly(lactic-co-glycolic acid) wafers for the localised treatment of glioblastoma multiforme: A comparison of manufacturing techniques. *J Pharm Sci* **104**:1076–1086.
62. Zhang R, Saito R, Mano Y, Sumiyoshi A, Kanamori M, Sonoda Y *et al* (2015) Convection-enhanced delivery of SN-38-loaded polymeric micelles (NK012) enables consistent distribution of SN-38 and is effective against rodent intracranial brain tumor models. *Drug Deliv* 1–7 [Epub ahead of print].
63. Zhou Y (2015) Application of acoustic droplet vaporization in ultrasound therapy. *J Ther Ultrasound* **3**:20.